Accounting for variability in ion current recordings using a mathematical model of artefacts in voltage-clamp experiments

Chon Lok Lei[1], Michael Clerx[1], Dominic G. Whittaker[2],
David J. Gavaghan[1], Teun P. de Boer[3] and Gary R. Mirams[2]

[1] Computational Biology & Health Informatics, Dept. of Computer Science, University of Oxford, UK.
[2] Centre for Mathematical Medicine & Biology, School of Mathematical Sciences, University of Nottingham, UK.
[3] Department of Medical Physiology, Division Heart & Lungs, University Medical Center Utrecht, Netherlands.

Abstract

Mathematical models of ion channels, which constitute indispensable components of action potential models, are commonly constructed by fitting to whole-cell patch-clamp data. In a previous study we fitted cell-specific models to hERG1a (Kv11.1) recordings simultaneously measured using an automated high-throughput system, and studied cell-cell variability by inspecting the resulting model parameters. However, the origin of the observed variability was not identified. Here we study the source of variability by constructing a model that describes not just ion current dynamics, but the entire voltage-clamp experiment. The experimental artefact components of the model include: series resistance, membrane and pipette capacitance, voltage offsets, imperfect compensations made by the amplifier for these phenomena, and leak current. In this model, variability in the observations can be explained by either cell properties, measurement artefacts, or both. Remarkably, assuming variability arises exclusively from measurement artefacts, it is possible to explain a larger amount of the observed variability than when assuming cell-specific ion current kinetics. This assumption also leads to a smaller number of model parameters. This result suggests that most of the observed variability in patch-clamp data measured under the same conditions is caused by experimental artefacts, and hence can be compensated for in post-processing by using our model for the patch-clamp experiment. This study has implications for the question of the extent to which cell-cell variability in ion channel kinetics exists, and opens up routes for better correction of artefacts in patch-clamp data.

1   Introduction

Mathematical modelling and computational simulations have been remarkably successful in providing mechanistic insight into many electrophysiological phenomena. Quantitative models of the action potential have demonstrated their usefulness in both basic research and safety-critical applications Mirams et al. (2012); Niederer et al. (2018); Li et al. (2019). Mathematical models of ion channels constitute indispensable components of these action potential models. Even when models are fitted to the best available data, uncertainty in their parameter values remains, which can be due to measurement uncertainty and/or physiological variability Mirams et al. (2016). Thus, identifying and quantifying the source of uncertainty is required prior to use of the models in safety-critical applications.

Whole cell patch-clamp voltage-clamp experiments are a common source of data for calibrating ion channel models. To study the dynamics of ion channels, currents through the cell membrane are often measured with a patch-clamp amplifier. In voltage-clamp mode, a patch-clamp amplifier is a sensitive feedback amplifier that rapidly calculates, applies and reports the small currents necessary to maintain a given voltage across a cell's membrane (and vice versa for current-clamp mode) Sigworth (1995b). Typically the current magnitudes are on the order of pA to µA, depending on the size of the cell, and the voltage across the cell membrane is usually on the order of tens of millivolts.

In our previous study Lei et al. (2019b), we performed a thorough analysis of hERG current kinetics simultaneously recorded in 124 cells using an automated high-throughput patch-clamp machine. The experiments used Chinese hamster ovary (CHO) cells stably expressing hERG1a. Since the cells expressed the same genes and were measured at the same time under highly similar conditions, one might expect the resulting current kinetics to be very similar across different cells. However, we observed a high level of variability, similar to that seen in previous studies using manual patch clamp experiments conducted

one cell at a time over several days Beattie et al. (2018). This raises a question — what is the origin of the observed variability?
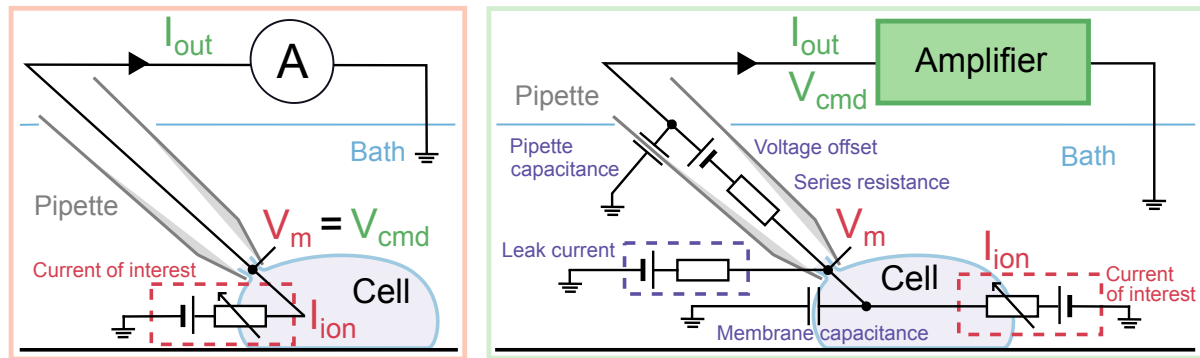

Figure 1: Schematics of the voltage-clamp experiment: **(left)** idealised and **(right)** more realistic. **Left:** Only the current of interest (red) is modelled. The membrane voltage, V_m (red) is assumed to be the same as the command voltage, V_{cmd} (green) set by the amplifier, and the observed current, I_{out} (green) is assumed to be equal to the ion channel current, I_{ion} (red). **Right:** Here, not only the current of interest (red) is modelled, but the patch-clamp amplifier process (green) and all of the experimental artefacts (purple) are included in the model. The differences between V_m (red) and V_{cmd} (green), and between I_{ion} (red) and I_{out} (green) are explicitly modelled in this framework.

Figure 1 (left) shows an idealised voltage-clamp experiment, where the cell is connected directly to an ammeter which records the current of interest, I_{ion}, while clamping the membrane to the command voltage, V_{cmd} (its equivalent circuit is shown Supplementary Figure S1). In other words, in a perfect patch clamp experiment

$$\text{(membrane voltage) } V_m = V_{cmd} \text{ (command voltage)}, \tag{1}$$

$$\text{(measured/observable current) } I_{out} = I_{ion} \text{ (current of interest)}. \tag{2}$$

Although the limitations of this idealised model are well-known, many studies assume the experimenter has compensated for any discrepancies (using specialised hardware, see below), so that the idealised assumptions can be used when analysing the experiments.

In voltage-clamp experiments, as illustrated in Figure 1 (right), the cell membrane acts as a capacitor in parallel to the ion currents. Between the electrode and the cell, there is a finite *series resistance* (MΩ), the effect of which is illustrated in Figure 3 of Marty & Neher Marty and Neher (1995). Furthermore, there is a voltage offset introduced at the electrode-cell junction Neher (1995), and the wall of the pipette (or the well plate in an automatic system) behaves as a capacitor. Finally, a finite seal resistance can cause a substantial leak current that contaminates the recording of the current of interest. All of these can be *partially* compensated by the patch-clamp amplifier using real-time hardware adjustments, or addressed in post-processing, and the remainder are what we term 'voltage-clamp experimental artefacts'.

In this paper, we relax the typical, ideal voltage-clamp assumptions by introducing a mathematical model for the voltage-clamp experiment, allowing and accounting for variability introduced by artefacts and their imperfect compensations in the experiments. The experimental artefact components of the model include the imperfect compensations made by the amplifier listed above, together with any residual uncompensated leak current. After deriving the mathematical model for the voltage-clamp experiment, we validate the mathematical model experimentally using electrical model cells, for which we designed a new type of electrical model cell which exhibits simple dynamics. Using this new mathematical model, variability in the observations can be explained by both cell properties as well as measurement artefacts. After the model validation, we develop an algorithm to optimise the ion current maximal conductance, the current kinetic parameters and the measurement artefact parameters at the same time. Finally, we compare and assess the performance of the models calibrated with the ideal voltage-clamp assumption and with the realistic voltage-clamp assumption. Whilst different cells certainly have varying maximal conductance of currents, the study has implications for the significance or even existence of cell-cell variability in ion channel kinetics, and opens up routes for better correction of artefacts in patch-clamp data.

Symbol	Typical values	Description
General		
t	—	Time variable
Capacitance		
C_f	$0.3\,\mathrm{pF}$	Feedback shunt capacitance
C_m	$5\text{–}20\,\mathrm{pF}$	Membrane capacitance (typical values for CHO cells only Lei et al. (2019b); can be up to $150\,\mathrm{pF}$ for cardiomyocytes O'Hara et al. (2011); or even $100\,\mathrm{nF}$ for *Xenopus laevis* oocytes Schmitt and Koepsell (2002))
C_p	$3\text{–}5\,\mathrm{pF}$	Parasitic capacitance at the electrode/pipette; also known as 'pipette capacitance' in manual patch
Current		
I_in	—	Voltage clamp current
I_inj	—	Injection current
I_ion	$\mathcal{O}(1)\,\mathrm{nA}$	Whole-cell ion channel current (can be up to $\mathcal{O}(1)\,\mu\mathrm{A}$ for *Xenopus laevis* oocytes Schmitt and Koepsell (2002))
I_leak	—	Leakage current through imperfect seal
I_m	—	Membrane current
I_out	—	Recorded current
I_p	—	Current drawn by parasitic capacitance of the electrode
Resistance		
R_f	$25\,\mathrm{M\Omega}$	Feedback resistance
R_s	$5\text{–}20\,\mathrm{M\Omega}$	Series resistance of the electrode
R_seal	$0.5\text{–}10\,\mathrm{G\Omega}$	Seal resistance of the pipette tip
Time constant		
τ_a	$50\text{–}2000\,\mu\mathrm{s}$	Membrane access time constant, $\tau_\mathrm{a} = R_\mathrm{s} C_\mathrm{m}$
τ_sum	$5\text{–}70\,\mu\mathrm{s}$	Response time of the summing amplifier
τ_clamp	$0.8\,\mu\mathrm{s}$	Voltage clamp time constant
τ_z	$7.5\,\mu\mathrm{s}$	Transconductor time constant, $\tau_\mathrm{z} = R_\mathrm{f} C_\mathrm{f}$
Voltage		
V_cmd	$\mathcal{O}(100)\,\mathrm{mV}$	Command voltage; follows the voltage clamp protocols
V_clamp	$\mathcal{O}(100)\,\mathrm{mV}$	Clamp voltage
V_m	$\mathcal{O}(100)\,\mathrm{mV}$	Membrane potential
V_off	$\mathcal{O}(10)\,\mathrm{mV}$	Offset voltage, such as amplifier offsets, electrode offsets, junction potentials, etc.
V_out	$\mathcal{O}(100)\,\mathrm{mV}$	Recorded voltage, $V_\mathrm{out} = I_\mathrm{out} R_\mathrm{f}$
V_p	$\mathcal{O}(100)\,\mathrm{mV}$	Pipette potential

Table 1: Glossary of symbols and parameters. We also denote the machine estimate of a parameter X as X^*, and the error in the estimate of the same parameter as $X^\dagger$. The range of typical values are taken from Weerakoon et al. (2009); Neher (1995), unless otherwise specified.

2 A detailed mathematical model of a voltage-clamp experiment

We present a more realistic equivalent circuit for a voltage-clamp set-up in Figure 2. Our goal is to observe the ion current across the cell membrane, I_ion. This current is present in the 'Cell Model' in Figure 2 (shown with black, dashed box). Between the Cell Model and the Headstage (green, dashed box) is where the pipette (or the well plate in an automatic system) sits, separating the cell membrane and the electrode, which includes many of the undesired artefact components shown in Figure 1 (right). There are five main undesired effects in this voltage-clamp set-up: 1. parasitic/pipette capacitance, 2. membrane capacitance, 3. series resistance, 4. voltage offset, 5. leak current. In Supplementary Section S2, we analyse each of these undesired effects and how they are typically compensated, to construct the voltage-clamp experiment model Moore et al. (1984); Neher (1992, 1995); Sigworth (1995a); Sigworth et al. (1995); Strickholm (1995); Sherman et al. (1999); Weerakoon et al. (2009, 2010). Table 1 contains a glossary of symbols and parameters used in this paper.

To model the dynamics of the current of interest, I_ion, we model the entire voltage-clamp experiment
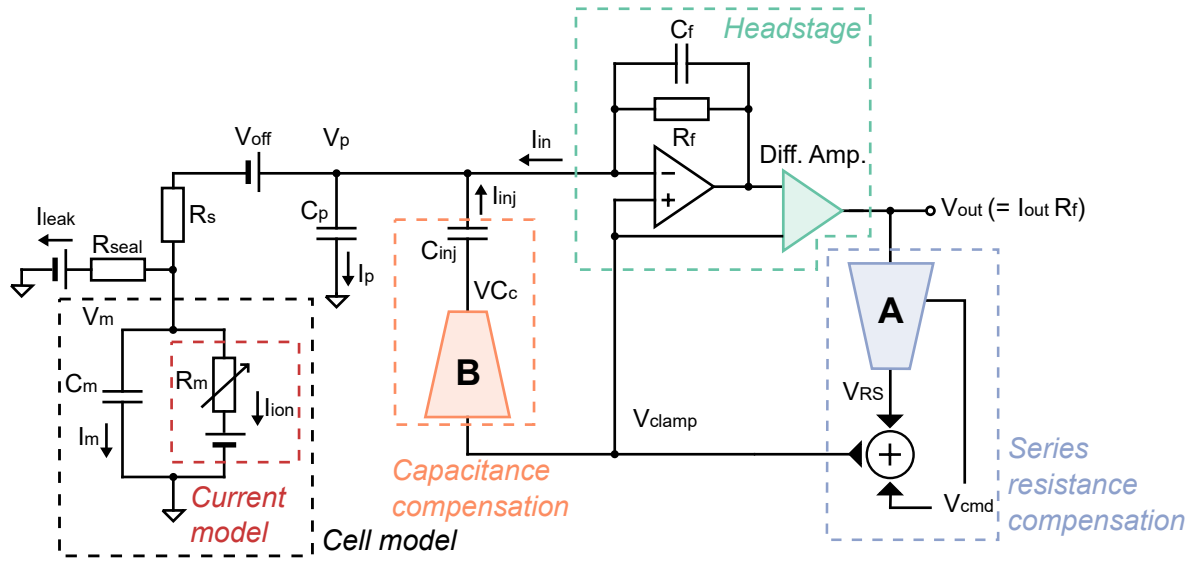
3

Figure 2: A more realistic voltage-clamp experiment equivalent circuit. This includes undesired factors such as voltage offset, series resistance between the electrode and the cell, cell capacitance, pipette capacitance, and leakage current, which can introduce artefacts to the recordings. The circuit also includes the components within a typical amplifier that are designed to compensate the artefacts. The blue **(A)** and orange **(B)** components are two idealised multiplying digital-to-analogue converters that control the amount of compensation. We assume that these, and the transimpedance amplifier and differential amplifier (green), to be ideal electrical components.

with the following set of equations:

$$I_{\mathrm{ion}} = f(t, V_{\mathrm{m}}), \qquad \text{Ion channel model} \qquad (3)$$

$$I_{\mathrm{leak}} = g_{\mathrm{leak}}\left(V_{\mathrm{m}} - E_{\mathrm{leak}}\right), \qquad \text{Leak current} \qquad (4)$$

$$\frac{\mathrm{d}V_{\mathrm{m}}}{\mathrm{d}t} = \frac{1}{R_{\mathrm{s}}C_{\mathrm{m}}}\left(V_{\mathrm{p}} + V_{\mathrm{off}}^{\dagger} - V_{\mathrm{m}}\right) \qquad \text{V_{off} compensation}$$

$$\qquad - \frac{1}{C_{\mathrm{m}}}\left(I_{\mathrm{ion}} + I_{\mathrm{leak}}\right), \qquad (5)$$

$$\frac{\mathrm{d}V_{\mathrm{p}}}{\mathrm{d}t} = \frac{1}{\tau_{\mathrm{clamp}}}\left(V_{\mathrm{clamp}} - V_{\mathrm{p}}\right), \qquad \text{Amplifier delay} \qquad (6)$$

$$\frac{\mathrm{d}V_{\mathrm{clamp}}}{\mathrm{d}t} = \frac{1}{\tau_{\mathrm{sum}}}\left(\left(V_{\mathrm{cmd}} + \alpha R_{\mathrm{s}}^{*}I_{\mathrm{out}}\right) - V_{\mathrm{clamp}}\right), \qquad \text{R_{s} compensation} \qquad (7)$$

$$I_{\mathrm{in}} = I_{\mathrm{ion}} + I_{\mathrm{leak}}$$

$$\qquad + C_{\mathrm{p}}\frac{\mathrm{d}V_{\mathrm{p}}}{\mathrm{d}t} - C_{\mathrm{p}}^{*}\frac{\mathrm{d}V_{\mathrm{clamp}}}{\mathrm{d}t} \qquad \text{C_{p} compensation}$$

$$\qquad + C_{\mathrm{m}}\frac{\mathrm{d}V_{\mathrm{m}}}{\mathrm{d}t} - C_{\mathrm{m}}^{*}\frac{\mathrm{d}V_{\mathrm{clamp}}}{\mathrm{d}t}, \qquad \text{C_{m} compensation} \qquad (8)$$

$$\frac{\mathrm{d}I_{\mathrm{out}}}{\mathrm{d}t} = \frac{1}{\tau_{\mathrm{z}}}\left(I_{\mathrm{in}} - I_{\mathrm{out}}\right). \qquad \text{Observed current} \qquad (9)$$

In these equations, α is the requested proportion of series resistance compensation (typically 70–80 %, a machine setting), and g_{leak} and E_{leak} are the conductance and the reversal potential of the leak current. Finally, I_{out} is then post-processed by subtracting $I_{\mathrm{leak}}^{*} = g_{\mathrm{leak}}^{*}(V_{\mathrm{cmd}} - E_{\mathrm{leak}}^{*})$. The meaning of the remaining symbols is given in Table 1. We also performed a local sensitivity analysis of the voltage-clamp experiment model to study the behaviour of the model, shown in Supplementary Section S3.

3 Validating the mathematical model with electrical model cell experiments

Before we apply the voltage-clamp experiment model to currents from a real biological cell, we test the performance of our mathematical model with *electrical model cells* — circuits made of electrical hardware components that mimic real cells. Some of these model cells are commercially available, and are used to test and calibrate patch-clamp amplifiers.

We are interested in both the current readout of a voltage-clamp and the clamped membrane voltage that the cell experiences. Therefore we designed a circuit that connects the model cell to two amplifiers, one in voltage-clamp mode and one in current-clamp mode, as shown in Figure 3. This set-up can simultaneously perform the conventional voltage-clamp procedure on the model cell with one amplifier; whilst using the other in current-clamp mode (clamped to zero) to measure the clamped voltage at the terminal corresponding to the membrane via the current-clamp. Effectively, this set-up allows us to record the membrane voltage V_{m} of the model cell whilst performing the conventional voltage-clamp measurements.

3.1 Electrical model cell design

Figure 3 (middle) shows the equivalent circuit of the standard commercially-available model cells, when under 'whole cell' mode. In this study, we call this a *Type I Model Cell*. It consists of a capacitor and a resistor in parallel to mimic the membrane capacitance, C_{m}, and membrane resistance, R_{m}. Unlike real ion channels, this simple electrical model cell lacks any current dynamics in the R_{m} resistor representing ion currents. We therefore developed a new type of model cell, termed a *Type II Model Cell*, which exhibits simple current dynamics when stepping to different voltages.

Figure 3 (right) shows the equivalent circuit of our Type II Model Cell. In addition to the usual C_{m} and R_{m} connected in parallel, this model cell has an extra component (R_{k} in series with C_{k}) connected in parallel, to mimic the addition of another ion current with some kinetic properties. The time constant ($\tau_k = R_{\mathrm{k}} C_{\mathrm{k}}$) for this extra component was chosen to be $\mathcal{O}(100)\,\mathrm{ms}$, which is of the same order of magnitude as I_{Kr} dynamics. The dynamics of the Type II Model Cell allow us to fully test and understand the effects of series resistance, etc. and their compensations, and enable us to verify our mathematical voltage-clamp experiment model experimentally.
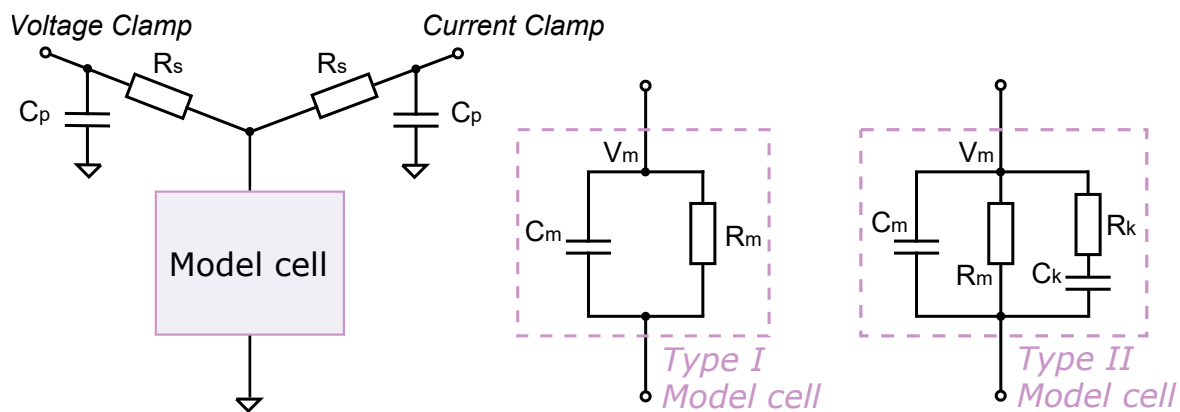

Figure 3: Circuit diagrams for model cell experiments. **(Left)** A circuit set-up where a model cell is connected to both a voltage-clamp amplifier and a current-clamp amplifier. The voltage-clamp imposes a command voltage, V_{cmd}, on the model cell and measures the current, I_{out}; while the current-clamp simultaneously measures its 'membrane voltage', V_{m}. **(Middle)** An equivalent circuit of the Type I Model Cell, which is identical to the commercial 'black box' model cells under the 'whole cell' mode. **(Right)** An equivalent circuit for the Type II Model Cell. This model cell is designed to exhibit dynamics when stepping to different voltages, with a time constant similar to ionic currents.

3.2 Validation of the mathematical model

The experimental recordings using the simultaneous voltage clamp-current clamp set-up (Figure 3) are shown in Figure 4 (solid lines), with Type I (A, C) and Type II (B, D) Model Cells. The measurements were performed with a holding potential at $0\,\mathrm{mV}$.

We performed two sets of experiments, firstly with no amplifier compensation, and secondly with automatic amplifier compensation using a computer controlled amplifier (HEKA EPC 10 Double Plus) where amplifier settings could be set with high precision. Here, automatic adjustment of the compensation settings, including V_{off}, C_{p}, C_{m}, and R_{s}, was performed using the HEKA Patchmaster software. This compensation is also commonly performed by hand on many manual patch-clamp amplifiers.

For the simulations, parameters were set in Eqs. (3–9) to correspond to each set of experiments: for no amplifier compensation, we set $\{V_{\mathrm{off}}^{\dagger}, C_{p}^{*}, C_{\mathrm{m}}^{*}, R_{\mathrm{s}}^{*}, g_{\mathrm{leak}}\}$ to zeros; while for the automatic amplifier compensation, those parameters were set to the amplifier's estimates. The results are shown in Figure 4 and Supplementary Figure S4.

Our model (dashed lines) is able to capture both the current and the membrane voltage very well, for all these experiments. Note the differences between the membrane voltage V_{m} (blue) and the command voltage V_{cmd} (orange/red), and how well our model is able to capture the details. For example, in the uncompensated case, due to the voltage drop across R_{s}, V_{m} exhibits nonlinear dynamics while V_{cmd} does not for Type II Model Cell; for Type I Model Cell, V_{m} shows a simple offset. Also, when the amplifier is actively compensating, the differences between V_{m} and V_{cmd} were successfully reduced. All of these details are captured excellently by our model. Therefore, we are confident that our voltage-clamp experiment model is a good representation of the voltage-clamp experiments and their artefacts.
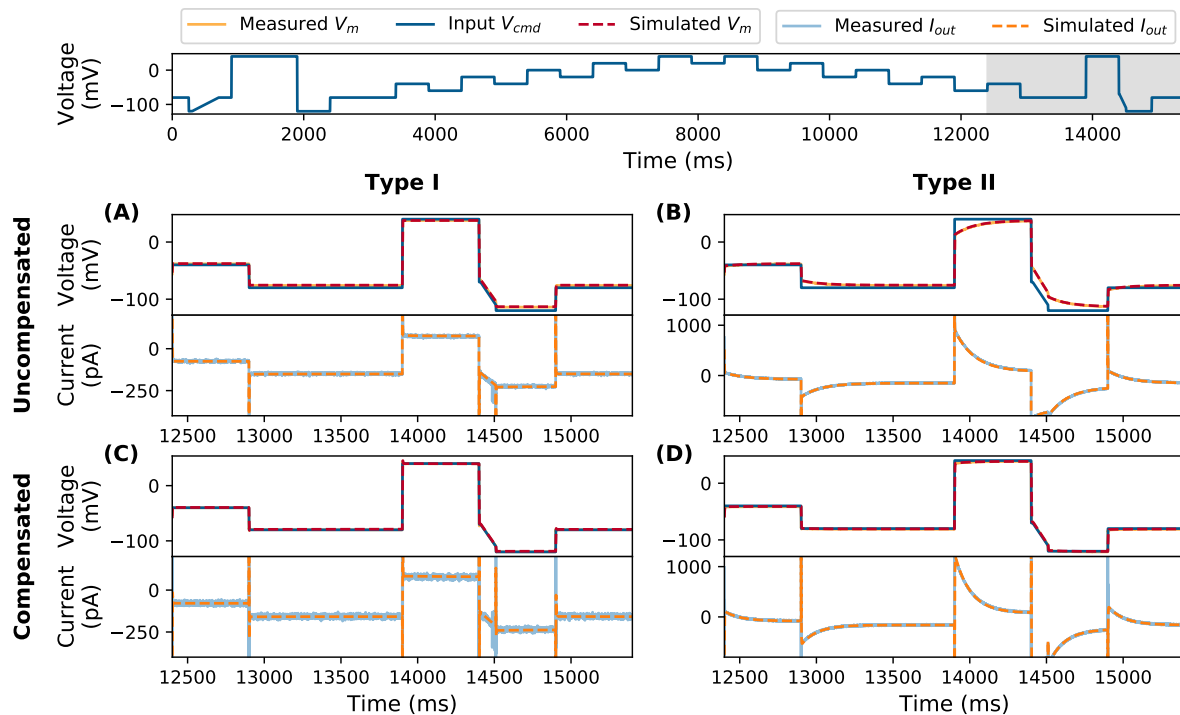

Figure 4: Model simulations (dashed lines) using the amplifier settings compared against the simultaneous voltage clamp-current clamp measurements of the model cells (solid lines). Measurements are shown without compensation using (**A**) Type I Model Cell and (**B**) Type II Model Cell; and measurements with automatic amplifier compensation for V_{off}, C_{p}, C_{m}, and R_{s} with $\alpha = 80\%$ using (**C**) Type I Model Cell and (**D**) Type II Model Cell. All command voltages were set to be the staircase voltage protocol Lei et al. (2019b) (top panel); here only the last $3\,\mathrm{s}$ of the measurement is shown, the whole trace is shown in Supplementary Figure S4. In the top panel of each subfigure, the blue lines represent the command voltage V_{cmd}, and the orange/red lines represent the membrane voltage V_{m}; the bottom panel shows the current readout via the voltage-clamp, I_{out}.

3.3 Parameter inference without compensations

Next, we attempt to use only the uncompensated, raw voltage-clamp measurements (i.e. only I_{out} in Figure 5A, and V_{cmd}) to infer the underlying membrane voltage, V_m, and the parameters of the model cells. We then compare the model V_m predictions with the current-clamp measurements. Here, we focus on the Type II Model Cell, since this should be the more challenging of the two and more similar to a real ionic current (similar results are shown for the Type I Model Cell in Supplementary Section S5). To optimise the model parameters we defined a root-mean-squared error (RMSE) between the simulated and recorded I_{out}, and then minimised it using a global optimisation algorithm Hansen (2006). All optimisation was done with an open source Python package, PINTS Clerx et al. (2019b), and simulations were performed in Myokit Clerx et al. (2016). All codes and data are freely available at https://github.com/CardiacModelling/VoltageClampModel.

Figure 5A shows the fitted model I_{out} (bottom, orange dashed line) and its corresponding prediction of the membrane voltage, V_m (top, red dashed line), compared against the experimental recordings (solid lines). Figure 5B further shows that the fitted model is able to predict measurements under an independent, unseen voltage-clamp protocol — a series of action potential waveforms (blue lines in the first panel) — very well. Note the excellent predictions for V_m in both cases.

Table 2 also shows a comparison of the values of the component labels (typical tolerances for these are ±1 to 2%) used in the electrical circuit hardware in Figure 3, the amplifier's estimation, and the fitted values using the mathematical model. Our model-inferred values are much closer to the component labels than the amplifier estimates. This is because our model cell, Type-II Model Cell, (or any realistic cell) exhibits nonlinear dynamics, whereas the amplifier uses a simple square-wave test pulse and assumes a simple resistor-capacitor model cell (Type-I Model Cell) to estimate the parameters. That is, there is a difference between the electrical model cell we attached and the circuit the amplifier is designed to compensate, thus leading to inaccurate estimation. For example, even though we did not apply any voltage offset, V_{off}, in the experiment, the amplifier incorrectly estimated an offset of $-1.2\,mV$. Proceeding with this amplifier-estimated value would lead to a voltage offset artefact of $V_{off}^\dagger = -1.2\,mV$ in all recordings.

	R_k (MΩ)	C_k (pF)	R_m (MΩ)	C_p (pF)	C_m (pF)	R_s (MΩ)	V_{off} (mV)
Component label	100	1000	500	4.7	22	30	0
Patchmaster estimate	—	—	91.30	8.80	41.19	33.60	-1.20
Fitted parameters	94.20	1062.69	520.70	4.85	36.38	34.87	0.20

Table 2: Type II Model Cell parameters (for the components shown in Figure 3), comparing the values on hardware component labels in the circuit (zero for V_{off} as there is no battery component), the values estimated by the Patchmaster amplifier software using a simple test pulse, and our inferred values from the mathematical model. The mathematical model can capture the fact that there are kinetics in the Type II cell and improve on the amplifier's estimates of the components.

Thus far, we considered a realistic voltage-clamp experiment and developed a detailed mathematical model for such a setting, where imperfect compensations made by the amplifier and imperfect leak current subtraction are included. We then validated this mathematical model via electrical model cell experiments, demonstrating that our model captures the effects of the voltage-clamp artefacts and amplifier compensations excellently. In the next part of the study, we apply our mathematical model to experimental CHO-hERG1a data recorded previously.

4 Application to CHO-hERG1a patch-clamp data

After experimentally validating our mathematical model of the full voltage-clamp experiment with two electrical model cells, we now apply it to experimental data from real cells. Here, we use a high-throughput dataset from our previous publication Lei et al. (2019b). The dataset contains 124 voltage-clamp recordings of the potassium current that flows through hERG (Kv11.1) channels (I_{Kr}) measured with a staircase protocol and eight other independent protocols. The measurements were performed on CHO cells stably transfected with hERG1a at 25 °C, using the Nanion SyncroPatch 384PE, a 384-well automated patch-clamp platform. For details of the experimental methods used, please see Lei et al. Lei et al. (2019b).
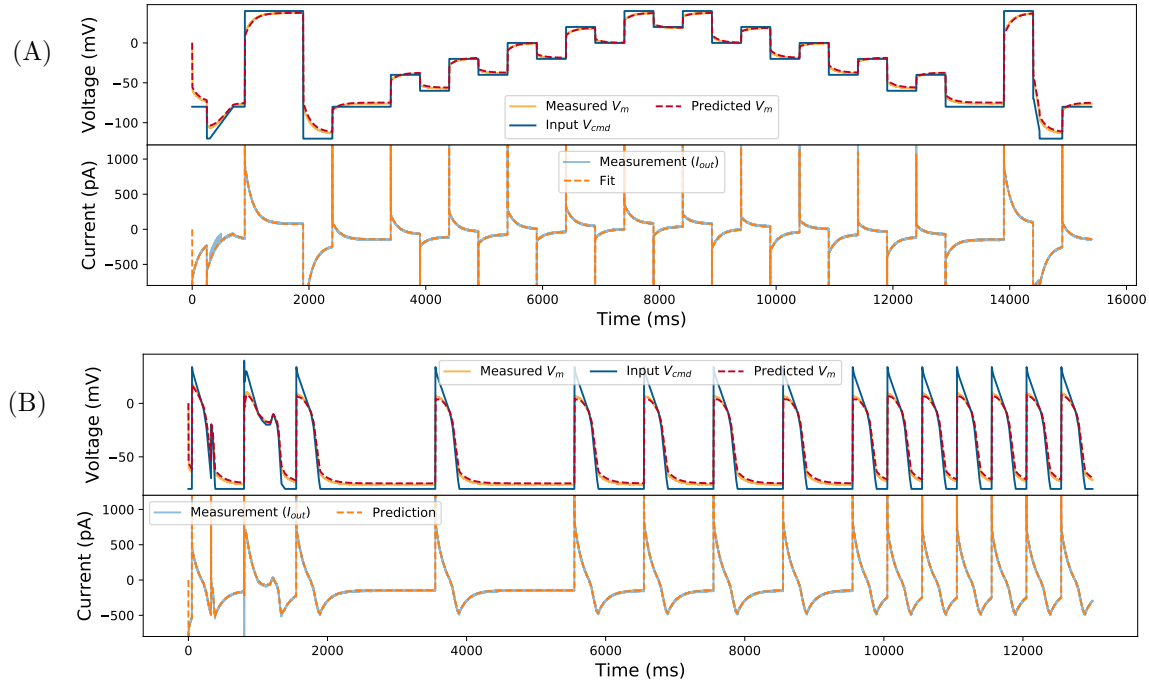
Figure 5: Inferred model simulations and predictions (dashed lines) compared to experimental data (solid lines) from a Type II Model Cell. **(A)** Model calibration with a staircase protocol (blue lines in the top panel), where the model was fitted to only the current recording (blue, solid line in the lower panel). The fitted model was able to predict the membrane voltage, V_{m} (orange, solid line) measured using current-clamp. **(B)** Further model validation using an independent voltage-clamp protocol, a series of action potentials (blue lines in the top panel). Again, predictions from the model fitted to the staircase protocol above (dashed lines) are excellent for both the current and the membrane voltage.

In the previous study Lei et al. (2019b), all of the observed variability was assumed to be due to biological variability in I_{Kr}, and so 124 cell-specific variants/parameterisations of the I_{Kr} model were created. Using this approach, we were able to show that fitting kinetic parameters to cell-specific data using the staircase protocol enabled very good predictions for the other eight independent validation protocols. However, covariance in the inferred parameters across cells led us to speculate about a voltage offset being responsible for much of the variability we saw Lei et al. (2019b). So an alternative hypothesis is that all cells have the same I_{Kr} kinetics, and that the observed variability is due to differences in the patch clamp artefacts and compensations for each cell. Figure 6 shows a schematic overview of the two hypotheses. We can now explore these hypotheses by fitting the same ion current kinetics parameters to every cell, but allowing the voltage-clamp model parameters to vary cell-to-cell.

4.1 A mathematical model of $I_{\mathbf{Kr}}$

We represented I_{Kr} using the same model as previously Beattie et al. (2018); Lei et al. (2019b,a); Clerx et al. (2019a). The current is described with two Hodgkin & Huxley-style gating variables (a for 'activation' and r for 'recovery' from inactivation) and a standard Ohmic expression,

$$I_{\mathrm{ion}} = I_{\mathrm{Kr}} = f(t, V_{\mathrm{m}}; g_{\mathrm{Kr}}, \boldsymbol{\theta}) = g_{\mathrm{Kr}} \cdot a \cdot r \cdot (V_{\mathrm{m}} - E_K), \tag{10}$$

where g_{Kr} is the maximal conductance, and E_K is the reversal potential (or Nernst potential) for potassium ions which can be calculated directly from concentrations either side of the membrane using the Nernst equation (Eq. 2 in Lei *et al.* Lei et al. (2019b)). The gates a and r are governed by the ordinary differential equations

$$\frac{\mathrm{d}a}{\mathrm{d}t} = \frac{a_\infty - a}{\tau_a}, \qquad\qquad \frac{\mathrm{d}r}{\mathrm{d}t} = \frac{r_\infty - r}{\tau_r}, \tag{11}$$
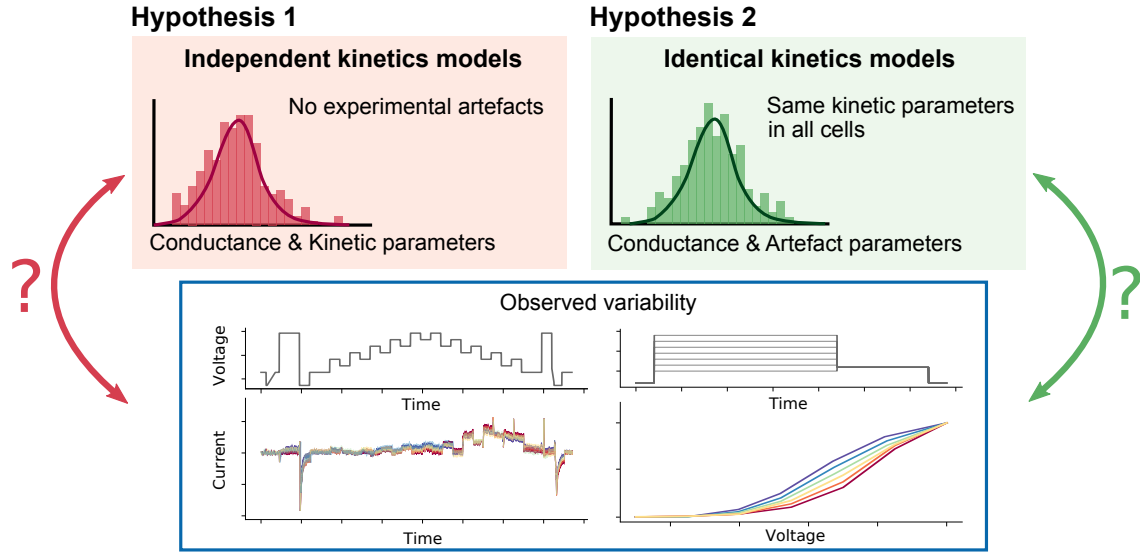
Figure 6: A schematic overview of the two hypotheses we explore. Hypothesis 1 (left) assumes a perfect, idealised voltage-clamp experiment where experimental artefacts are absent, and all the observed variability is rooted in biological variability (varying conductance and model kinetics in every cell), we term these 'independent kinetics models'. Hypothesis 2 (right) assumes that the observed variability is due to differences in the voltage-clamp experimental artefacts, and that all of the cells share identical ion channel kinetics (although the maximum conductance is allowed to vary across cells), we term these 'identical kinetics models'.

with

$$a_\infty = \frac{k_1}{k_1 + k_2}, \qquad\qquad r_\infty = \frac{k_4}{k_3 + k_4}, \qquad (12)$$

$$\tau_a = \frac{1}{k_1 + k_2}, \qquad\qquad \tau_r = \frac{1}{k_3 + k_4}, \qquad (13)$$

and

$$k_1 = p_1 \exp(p_2 V_\mathrm{m}), \qquad\qquad k_3 = p_5 \exp(p_6 V_\mathrm{m}), \qquad (14)$$

$$k_2 = p_3 \exp(-p_4 V_\mathrm{m}), \qquad\qquad k_4 = p_7 \exp(-p_8 V_\mathrm{m}). \qquad (15)$$

The model has 9 positive parameters, g_Kr and $\boldsymbol{\theta} = \{p_1, p_2, \cdots, p_8\}$, where the units of the parameters are $\{\mathrm{pS}, \mathrm{s}^{-1}, \mathrm{V}^{-1}, \mathrm{s}^{-1}, \cdots\}$. All 9 parameter values are optimised to fit the experimental data.

4.2 Combining the models of voltage-clamp artefacts and I_Kr

Before moving on to test the two hypotheses shown in Figure 6, we show how our voltage-clamp experiment model performs when combined with the I_Kr model of Eq. (10). We first tested the entire model with synthetic data studies shown in Supplementary Section S6, in which we were able to identify all of the parameters (model parameters g_Kr and $\boldsymbol{\theta}$ together with artefact parameters C_m, C_p, R_s, $V_\mathrm{off}^\dagger$ and g_leak). We then tested the model with the experimental data from our previous study Lei et al. (2019b). However, unlike in the synthetic data studies, values of the series resistance, R_s, were consistently estimated at the lower bound we had imposed. We believe this is due to the imperfect representation of real I_Kr by the model, as we sucessfully tested both the parameter inference scheme with synthetic data, and the voltage-clamp experiment model with electrical model cell experiments. We therefore propose a simplification of the voltage-clamp experiment model while capturing the principal causes of variability.

4.3 A simplified voltage-clamp experiment model

Modelling the whole voltage clamp machine can be difficult, because the timescales of the components in the system span multiple orders of magnitude; ranging from fractions of a µs (e.g. τ_clamp) to tens of ms (e.g. 'C-slow') or even tens of seconds for ion channels (e.g. activation of I_Kr). For our investigations

9

here, I_{Kr} measurements (and their variability), we approximate the two fastest processes, τ_{clamp} and τ_{z}, as instantaneous responses. That is, we assume Eqs. (6) & (9) can be approximated as $V_{\mathrm{p}} \approx V_{\mathrm{clamp}}$ and $I_{\mathrm{out}} \approx I_{\mathrm{in}}$, respectively.

After analysing the local sensitivity of the voltage-clamp experiment model (Supplementary Section S3), we found that the effects of $V_{\mathrm{off}}^{\dagger}$ and imperfect R_{s} compensation are most apparent in the observed current (on timescales relevant to I_{Kr}). As a result, we further assume that 1. τ_{sum}, part of the fast amplifier processes, is instantaneous; 2. the effects of C_{p} and C_{m} are negligible; and 3. $C_{\mathrm{m}}^{*}, R_{\mathrm{s}}^{*} \approx C_{\mathrm{m}}, R_{\mathrm{s}}$. Finally, the data were leak subtracted, where the leak current parameters (g_{leak}^{*} and E_{leak}^{*}) were estimated by fitting Eq. (4) to current around the -120 to $-80\,\mathrm{mV}$ leak-ramp at the beginning of the measurements, yielding zero current at holding potential Lei et al. (2019b). We allow for this leak subtraction being imperfect by retaining a small residual leak current with parameters $g_{\mathrm{leak}}^{\dagger}$ and $E_{\mathrm{leak}}^{\dagger}$.

With these assumptions, Eqs. (3)–(9) become

$$I_{\mathrm{ion}} = f(t, V_{\mathrm{m}}; g_{\mathrm{Kr}}, \boldsymbol{\theta}) = I_{\mathrm{Kr}}, \qquad \text{Ion channel model} \qquad (16)$$

$$I_{\mathrm{leak}} = g_{\mathrm{leak}}^{\dagger}\left(V_{\mathrm{m}} - E_{\mathrm{leak}}^{\dagger}\right), \qquad \text{Residual leak current} \qquad (17)$$

$$\frac{\mathrm{d}V_{\mathrm{m}}}{\mathrm{d}t} = \frac{1}{R_{\mathrm{s}}^{*} C_{\mathrm{m}}^{*}}\left(V_{\mathrm{p}} + V_{\mathrm{off}}^{\dagger} - V_{\mathrm{m}}\right) - \frac{1}{C_{\mathrm{m}}^{*}} I_{\mathrm{ion}}, \qquad V_{\mathrm{off}} \text{ compensation} \qquad (18)$$

$$V_{\mathrm{p}} = V_{\mathrm{cmd}} + \alpha R_{\mathrm{s}}^{*} I_{\mathrm{out}}, \qquad R_{\mathrm{s}} \text{ compensation} \qquad (19)$$

$$I_{\mathrm{out}} = I_{\mathrm{ion}} + I_{\mathrm{leak}}. \qquad \text{Observed current} \qquad (20)$$

For all symbols refer to Table 1. Here, we have only two voltage-clamp model parameters ($V_{\mathrm{off}}^{\dagger}$ and $g_{\mathrm{leak}}^{\dagger}$) to infer along with the ion current parameters (g_{Kr} and $\boldsymbol{\theta}$). Note that the other parameters (α, C_{m}^{*}, and R_{s}^{*}) can be obtained from the amplifier settings without performing inference. The effective reversal potential of the residual leak current, $E_{\mathrm{leak}}^{\dagger}$, is chosen to be the holding potential ($-80\,\mathrm{mV}$) because the primary leak-subtraction (fit of g_{leak}^{*} and E_{leak}^{*}) ensured approximately zero current at holding potential.

This simplified voltage-clamp experiment model is applied to the model cell experiments, and the results are shown in Supplementary Section S7. We show that the simplified voltage-clamp experiment model is able to correct the imperfect compensations made by the amplifier.

4.4 Optimisation of model parameters

We now present the parameter optimisation schemes used to test each hypothesis.

4.4.1 Hypothesis 1: Cell-specific kinetics with no artefacts

Hypothesis 1 (Figure 6, left) assumes a perfect, idealised voltage-clamp experiment, as shown in Figure 1 (left). In this hypothesis, there are no experimental artefacts, so models fitted to the recorded current should show variability in the obtained kinetic parameters, which reflects underlying variability in the biology. To test this hypothesis, we employ the parameter inference scheme detailed in Lei *et al.* Lei et al. (2019b). In summary, we used a Bayesian inference scheme which resulted in very narrow distributions. This scheme used some parameter transforms so that the optimisation algorithm Hansen (2006) searches in log-transformed space for certain parameters Clerx et al. (2019a). Here we look for the most likely parameter set under that scheme, which is identical to that given by a least square-error fit. So the likelihood L_i of a given parameter set for cell i is proportional to

$$L_i = -\sum\left(I_i^{\mathrm{model}} - I_i^{\mathrm{data}}\right)^2. \qquad (21)$$

Under this hypothesis, I_i^{model} is a function of just conductance g_i and kinetic parameters $\boldsymbol{\theta}_i$, and is given by Eq. (10) while assuming $V_{\mathrm{m}} = V_{\mathrm{cmd}}$. So we performed an optimisation to maximise L_i by finding g_i and $\boldsymbol{\theta}_i$ for each cell i independently. We termed the resulting mathematical models under this hypothesis the '*independent kinetics models*'.

4.4.2 Hypothesis 2: Identical kinetics for all cells, with cell-specific artefacts

Hypothesis 2 (Figure 6, right) assumes that the observed variability is due to the imperfect voltage-clamp experiments. Under this assumption, models fitted to the data should have the same kinetic parameters,

$\boldsymbol{\theta}^*$, across all cells, that is, $\boldsymbol{\theta}_i = \boldsymbol{\theta}^*$ for any cell i, . But there will be a cell-specific I_{Kr} conductance, g_i, and different patch-clamp experiment parameters for each cell too, $\boldsymbol{\phi}_i = \{V_{\mathrm{off},i}^\dagger, g_{\mathrm{leak},i}^\dagger\}$. We termed these models the '*identical kinetics models*'.

To impose the assumption that all N cells have the same kinetics, and that the observed variability arises only from the experimental artefacts, the likelihood becomes

$$\mathcal{L}\left(\boldsymbol{\theta}, \{g_1, \ldots, g_N, \boldsymbol{\phi}_1, \ldots, \boldsymbol{\phi}_N\}\right) = \prod_{i=1}^{N} L_i\left(\boldsymbol{\theta}, g_i, \boldsymbol{\phi}_i\right), \tag{22}$$

where L_i, defined by Eq. (21), is the likelihood for the ith cell. Under this hypothesis, I_i^{model} is the observed current I_{out} in Eq. (20) and hence L_i is a function of the artefact parameters $\boldsymbol{\phi}_i$ too.

Optimising $\mathcal{L}$ is a high-dimensional optimisation problem, which is computationally expensive. We reduce this burden with a Gibbs-sampling style scheme; we break the optimisation problem into two: i) optimising the common kinetics parameters, $\boldsymbol{\theta}$; and ii) optimising the cell-specific parameters, $\{g_i, \boldsymbol{\phi}_i\}_{i=1,\ldots,N}$. To evaluate the maximum likelihood of $\boldsymbol{\theta}$, we nest optimisation schemes. That is, for any single estimate of $\boldsymbol{\theta}$, we optimise $\{g_i, \boldsymbol{\phi}_i\}$ for each cell i *independently* to compute an approximate likelihood for $\boldsymbol{\theta}$. The estimate of $\boldsymbol{\theta}$ is then updated by running a single iteration of the outer optimisation loop, followed again by optimisation to convergence for $\{g_i, \boldsymbol{\phi}_i\}$ in each cell. When this overall scheme converges we obtain the full set of optimal parameters: $\boldsymbol{\theta}^*, \{g_i^*, \boldsymbol{\phi}_i^*\}_{i=1,\ldots,N}$. The algorithm is detailed in Supplementary Material S8.

4.5 Variability in ion channel kinetics or variability in patch-clamp artefacts?

We next compare the performance of the models arising from the two hypotheses. For Hypothesis 1, the independent kinetics models, we directly use the results from Lei *et al.* Lei et al. (2019b), as it assumes there were no artefacts and all the variability was the result of kinetic variability. For Hypothesis 2, the identical kinetics models, we use the results from optimising $\mathcal{L}(\boldsymbol{\theta})$ in Eq. (22). The optimised parameters, steady state-voltage relations, and time constants-voltage relations for the new identical kinetics models are shown in Supplementary Section S9.

As previously Lei et al. (2019b), we quantified the fits and predictions using relative root mean square error (RRMSE), defined as the root mean square error between the model simulation and the experimental data, divided by the root mean square distance of the data to a zero current trace:

$$\mathrm{RRMSE} = \sqrt{\sum \left(I^{\mathrm{model}} - I^{\mathrm{data}}\right)^2 \Big/ \sum \left(I^{\mathrm{data}}\right)^2}. \tag{23}$$

Using this RRMSE quantification, the difference in the absolute size of the current across cells due to varying conductance is eliminated such that the scores are comparable between cells.
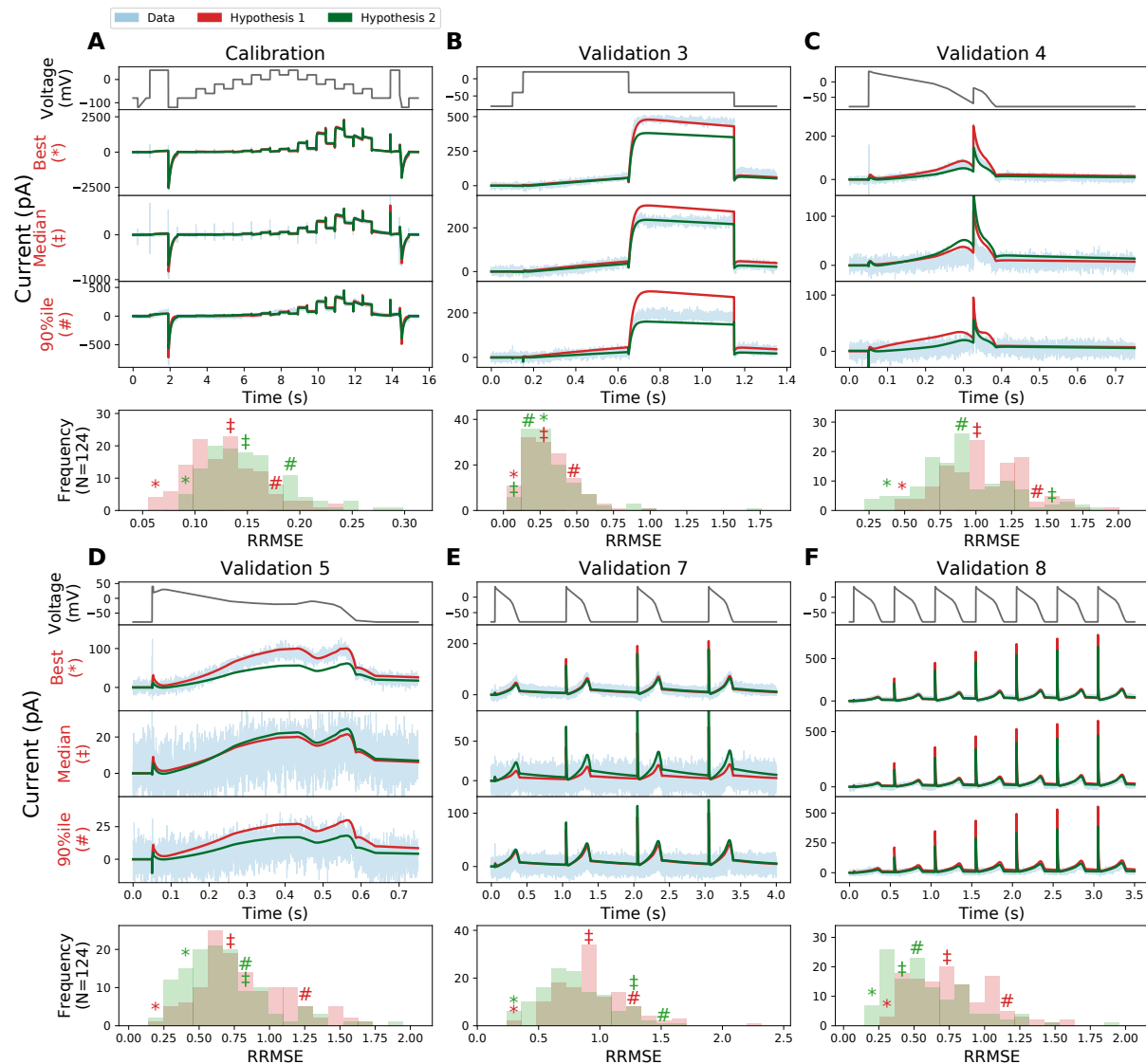
Figure 7 shows the RRMSE histograms for all 124 cells, for six different protocols, and for the two sets of models. Markers indicate the best ($*$), median ($\ddagger$) and 90th percentile ($\#$) RRMSE values for the independent kinetics models (red), and the corresponding raw traces are shown in the three panels above. The model predictions for the same 3 cells with the identical kinetics model are shown in green.

For the calibration, shown in Figure 7A, it is clear that the RRMSE histogram of the independent kinetics models (red) is better than the identical kinetics models (green). This is not unexpected, as the independent kinetics model has 9 parameters to fit each experiment while the identical kinetics model has only 3 parameters. In other words, the independent kinetics models have more degrees of freedom to fit to the data, hence they are more likely to get a better fit. However, this could also lead to overfitting, as discussed below. For the validations/predictions (Figure 7B–F), it is surprising to see that the identical kinetics assumption performs slightly better than independent kinetics.

In the identical kinetics models, all the variability is explained by the voltage clamp artefact parameters, $\boldsymbol{\phi}_i$, in Eq. (22). Figure 8 shows the histograms and the pairwise scatter plots of the obtained $\{g_{\mathrm{Kr},i}^*, \boldsymbol{\phi}_i^*\}_{i=1,\ldots,124}$. The artefact parameter values are within reasonable ranges: $\sim \pm 5\,\mathrm{mV}$ for $V_{\mathrm{off}}^\dagger$ and $g_{\mathrm{leak}}^\dagger \ll g_{\mathrm{Kr}}$. The fact that the identical kinetics hypothesis predicts the validation protocol results slightly better than the independent kinetics whilst using far fewer parameters ($124 \times 3 + 8 = 380$ compared to $124 \times 9 = 1116$) may be a sign of overfitting, and strongly suggests that identical kinetics is the leading hypothesis for these data.

Note that Hypothesis 2 results in a slightly different set of 'consensus' kinetic parameters to the mean of the independently-fitted parameter sets from Hypothesis 1 — as a nonlinear effect is introduced by

11

the artefacts that are present (under Hypothesis 2) in the data. In Supplementary Section S9 we list these parameter sets and compare model properties for the two approaches.
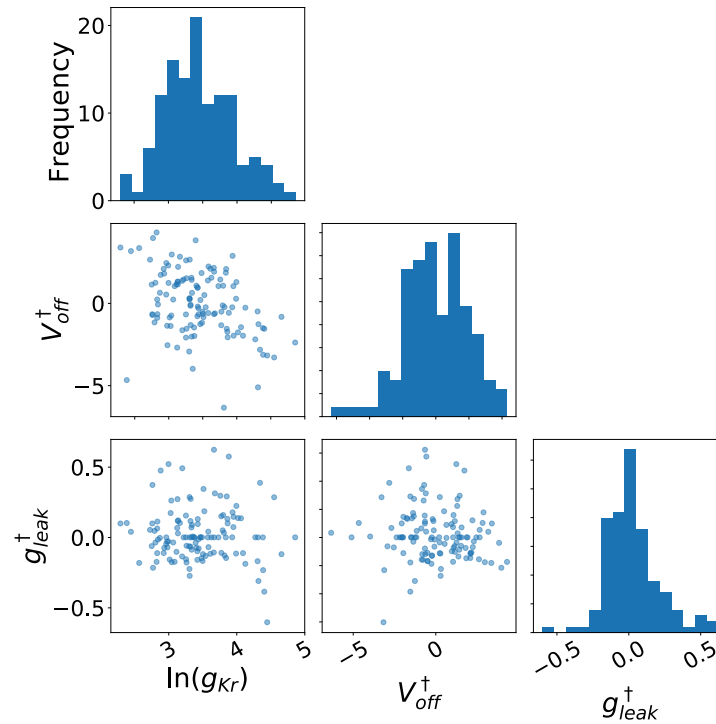

Figure 7: The relative root mean square error (RRMSE) histograms for 6 protocols, comparing the independent kinetics models from Lei *et al.* Lei et al. (2019b) and the identical kinetics models with voltage-clamp artefact. Each histogram represents the same 124 cells with a different protocol and RRMSE each time. Red markers indicate the best (∗), median (‡) and 90th percentile (#) RRMSE values for the independent kinetics model; green markers are the same cell prediction from the identical kinetics models. For each protocol, the raw traces for the identical kinetics model (green), the independent kinetics model (red), and data (blue) are shown, with the voltage-clamp above. Note that the currents are shown on different scales, to reveal the details of the traces. The same analysis applied to the remaining 3 protocols is shown in Supporting Material. Quantitatively, the two models show a similar RRMSE distribution for each protocol, with a slightly larger error on average in the fit for the identical kinetics (A), but a slightly lower error in predictions. In particular, note how the errors seen in the cell-specific predictions (shown by red traces) in panel B are almost perfectly explained by the identical kinetics model (green).

12

Figure 8: The inferred voltage-clamp artefact parameters across experimental wells. Each of the parameters exhibits a Gaussian-like distribution under a proper choice of transformation. The artefact parameter values are within reasonable ranges: $V_{\text{off}}^{\dagger} \sim \pm 5\,\text{mV}$ and $g_{\text{leak}}^{\dagger} \ll g_{\text{Kr}}$.

5 Discussion

In this paper we have introduced a new mathematical model for voltage-clamp experiments that allows and accounts for experimental artefacts and imperfect compensations of these artefacts, as well as imperfections in leak current subtraction. We validated the mathematical model through experiments using two types of electrical model cells, where we showed that our mathematical model is able to rectify imperfect amplifier estimations. This is, to our knowledge, the first time a detailed voltage-clamp experiment model has been used for parameter optimisation in ion channel modelling.

Patch-clamp data show a high-level of variability Zhou et al. (1998); Vandenberg et al. (2006); Beattie et al. (2018); Lei et al. (2019b,a), with differences in observed current kinetics between experiments. The current that we observe is the whole-cell 'macroscopic' current, which one might expect to vary with stochastic ion channel activity. But we have observed it to be reproducible within a given cell Lei et al. (2019b,a) — that is, the variability upon repeats in the same cell at different moments in time is much smaller than the cell-to-cell variability. We do expect the maximum *conductance* of the current to differ between cells, due to varying cell sizes and gene expression levels. But since each cell expresses the same channel gene, there is no immediately obvious reason for the current *kinetics* to vary cell-to-cell, especially if the cells are from the same culture and recorded simultaneously under very similar conditions as they were in our high-throughput data.

Each voltage-clamp experiment has a different cell membrane capacitance, pipette (or well plate in automated clamp) capacitance, voltage offset, series resistance, and leak current. This has led us to propose two competing hypotheses in Figure 6: Hypothesis 1, cell-specific kinetics with no artefacts; and Hypothesis 2, identical kinetics for all cells with cell-specific artefacts. A parameter optimisation technique was developed for Hypothesis 2, so that we were able to optimise all the model parameters at once (cell-specific conductances and measurement artefact parameters, with a single set of kinetic parameters shared by all the cells).

After analysing the two hypotheses, it is more plausible that the observed variability arises from patch-clamp experimental artefacts: imperfect amplifier compensations and imperfect leak current subtraction. This is because the mathematical model with fewer parameters, i.e. the simpler model, made better predictions, on average, over all the cells we analysed. Considering Occam's razor, this makes the 'identical kinetics' hypothesis, in which fewer assumptions are made, the favourable explanation. The

13

findings support a hypothesis that the kinetics of currents may be identical across cells, as one might expect since the ion channel proteins that conduct the currents are the same, especially in our over-expression cell line. We should mention that these results and this interpretation are specific to our preparation though. In native myocytes, differing subunit expression and other signalling-related changes in proteins' states in the membrane could also confer some variability in kinetics from cell-cell. But this study suggests a major, if not the only, factor causing apparent variability in kinetics will be artefacts introduced by the patch-clamp experimental procedure, and offers an approach to address it.

Determining the origin of variability is particularly important for forward propagation of uncertainty in cardiac modelling. Unified ion channel kinetics provide a sensible way of constructing cardiac action potential models. If each ion current biologically exhibited a high-degree of variability in the observed patch-clamp data, then samples of this variability for all currents would be necessary. However, if the majority of the variability is due to experimental artefacts, the standard approach to building action potential models with a single set of kinetic parameters for each current is sensible Ten Tusscher et al. (2004); O'Hara et al. (2011); Groenendaal et al. (2015); Lei et al. (2017), and we do not need to propagate the observed cell-cell variability in kinetics data forward (as some authors have Pathmanathan et al. (2015)). Nevertheless, we may still need an approach like the one demonstrated here to determine unbiased ion channel kinetics (rather than taking the mean of biased recordings which would accidentally include experimental artefacts within the models, see Supplementary Section S9) to build the most physiologically-relevant action potential models.

Identifying ion current kinetics and separating out experimental artefacts is crucial for many cardiac electrophysiology studies. For example, ion channel mutation studies often conclude with a statement like "there is a 5–10 mV shift in the half-activation potential" Clerx et al. (2018); Ng et al. (2019). However, given the variability that we observe in patch-clamp data, often the variability in half-activation potential can be in the range of 10–15 mV. Therefore, it is important to separate out experimental artefacts from real biological effects. The same principle applies to other cardiac electrophysiology studies, such as drug studies and the basic ion channel characterisation.

The findings raise the question of whether a mathematical model of the voltage clamp experiment could remove the need for amplifier compensations altogether: this works well when we have an almost perfect model of the current, as in the electrical model cell case (see Figure 5). But care should be taken in situations where we are dealing with an imperfect model for the ionic current, where it is possible for the artefact model to (erroneously) fit some parts of the ionic current, as we may have seen in Section 44.2. Still, our simplified voltage-clamp model appears to account well for small artefacts in the applied voltage clamp even with an imperfect model of I_{Kr} kinetics.

In this study we have demonstrated that a voltage-clamp experiment model can unify the kinetics of I_{Kr} measured across many cells. Our voltage-clamp experiment model is general and can be applied to study variability in any whole-cell ion current patch-clamp data Bekkers et al. (1990); Finkel et al. (2006); Feigenspan et al. (2010); Golowasch (2014); Santillo et al. (2014); Altomare et al. (2015); Annecchino and Schultz (2018). Our full model of the voltage-clamp experiment could be particularly useful for currents like the fast sodium current (I_{Na}) where the time constants are similar to those in the capacitance artefacts. Although currently the full voltage-clamp experiment model with the I_{Kr} model suffers from discrepancy (a difference between the model and reality) when applying it to the dataset from Lei et al. (2019b), we envision that an improved I_{Kr} model or techniques for accounting for discrepancy Lei et al. (2020) will allow us to infer parameters for all experimental artefacts. Finally, it should be possible to generalise our method to current-clamp experiments.

6   Conclusions

In this study, we have derived a mathematical model that describes the entire voltage-clamp experiment including artefacts, imperfect amplifier compensations, and imperfect leak current subtraction. Using this model, variability in experimental observations could be explained either by varying current properties or varying measurement artefacts. After comparing the performance of the models calibrated with a varying kinetics assumption with an identical kinetics assumption, the results suggest that most of the observed variability in our patch-clamp data measured under the same conditions is caused by experimental artefacts. These varying experimental artefacts can be compensated for in post-processing by fitting our mathematical model for the patch-clamp experiment at the same time as fitting ion channel kinetics. This study raises questions for the biological significance of any cell-cell variability in macroscopic ion channel kinetics, and provides for better correction of artefacts in patch-clamp data.

Data access

All codes and data are freely available at
https://github.com/CardiacModelling/VoltageClampModel.

Author contributions

CLL & DGW built the model cells and carried out the experiments. CLL, MC & GRM derived the mathematical models. CLL wrote code for and performed the simulations and data analysis, and generated the results figures. CLL, MC, DJG, TPdB and GRM conceived of and designed the study. All authors drafted and approved the final version of the manuscript.

Competing interests

The authors declare that they have no competing interests.

Funding

Acknowledgements

References

Altomare, C., Bartolucci, C., Sala, L., Bernardi, J., Mostacciuolo, G., Rocchetti, M., Severi, S., Zaza, A., 2015. IKr impact on repolarization and its variability assessed by dynamic clamp. Circulation: Arrhythmia and Electrophysiology 8, 1265–1275.

Annecchino, L.A., Schultz, S.R., 2018. Progress in automating patch clamp cellular physiology. Brain and Neuroscience Advances 2, 2398212818776561.

Beattie, K.A., Hill, A.P., Bardenet, R., Cui, Y., Vandenberg, J.I., Gavaghan, D.J., De Boer, T.P., Mirams, G.R., 2018. Sinusoidal voltage protocols for rapid characterisation of ion channel kinetics. The Journal of physiology 596, 1813–1828.

Bekkers, J., Richerson, G., Stevens, C., 1990. Origin of variability in quantal size in cultured hippocampal neurons and hippocampal slices. Proceedings of the National Academy of Sciences 87, 5359–5362.

Clerx, M., Beattie, K.A., Gavaghan, D.J., Mirams, G.R., 2019a. Four ways to fit an ion channel model. Biophyical Journal 117, 2420–2437.

Clerx, M., Collins, P., de Lange, E., Volders, P.G.A., 2016. Myokit: A simple interface to cardiac cellular electrophysiology. Progress in Biophysics and Molecular Biology 120, 100–114.

Clerx, M., Heijman, J., Collins, P., Volders, P.G., 2018. Predicting changes to INa from missense mutations in human SCN5A. Scientific reports 8, 12797.

Clerx, M., Robinson, M., Lambert, B., Lei, C.L., Ghosh, S., Mirams, G.R., Gavaghan, D.J., 2019b. Probabilistic inference on noisy time series (PINTS). Journal of Open Research Software 7, 23.

Feigenspan, A., Dedek, K., Schlich, K., Weiler, R., Thanos, S., 2010. Expression and biophysical characterization of voltage-gated sodium channels in axons and growth cones of the regenerating optic nerve. Investigative ophthalmology & visual science 51, 1789–1799.

Finkel, A., Wittel, A., Yang, N., Handran, S., Hughes, J., Costantin, J., 2006. Population patch clamp improves data consistency and success rates in the measurement of ionic currents. Journal of biomolecular screening 11, 488–496.

Golowasch, J., 2014. Ionic current variability and functional stability in the nervous system. Bioscience 64, 570–580.

Groenendaal, W., Ortega, F.A., Kherlopian, A.R., Zygmunt, A.C., Krogh-Madsen, T., Christini, D.J., 2015. Cell-specific cardiac electrophysiology models. PLoS computational biology 11, e1004242.

Hansen, N., 2006. The CMA Evolution Strategy: A Comparing Review. Springer Berlin Heidelberg, Berlin, Heidelberg. pp. 75–102.

Lei, C.L., Clerx, M., Beattie, K.A., Melgari, D., Hancox, J.C., Gavaghan, D.J., Polonchuk, L., Wang, K., Mirams, G.R., 2019a. Rapid characterisation of hERG channel kinetics II: temperature dependence. Biophysical Journal 117, 2455–2470.

Lei, C.L., Clerx, M., Gavaghan, D.J., Polonchuk, L., Mirams, G.R., Wang, K., 2019b. Rapid characterisation of hERG channel kinetics I: using an automated high-throughput system. Biophysical Journal 117, 2438–2454.

Lei, C.L., Ghosh, S., Whittaker, D.G., et al., 2020. Accounting for discrepancy when calibrating a mechanistic electrophysiology model. Philosophical Transactions of the Royal Society A this volume.

Lei, C.L., Wang, K., Clerx, M., Johnstone, R.H., Hortigon-Vinagre, M.P., Zamora, V., Allan, A., Smith, G.L., Gavaghan, D.J., Mirams, G.R., Polonchuk, L., 2017. Tailoring mathematical models to stem-cell derived cardiomyocyte lines can improve predictions of drug-induced changes to their electrophysiology. Frontiers in Physiology 8.

Li, Z., Ridder, B.J., Han, X., Wu, W.W., Sheng, J., Tran, P.N., Wu, M., Randolph, A., Johnstone, R.H., Mirams, G.R., et al., 2019. Assessment of an in silico mechanistic model for proarrhythmia risk prediction under the CiPA initiative. Clinical Pharmacology & Therapeutics 105, 466–475.

Marty, A., Neher, E., 1995. Tight-seal whole-cell recording, in: Sakmann, B., Neher, E. (Eds.), Single-Channel Recording. Springer US, Boston, MA. chapter 6, 2 edition. pp. 31–52.

Mirams, G.R., Davies, M.R., Cui, Y., Kohl, P., Noble, D., 2012. Application of cardiac electrophysiology simulations to pro-arrhythmic safety testing. British journal of pharmacology 167, 932–945.

Mirams, G.R., Pathmanathan, P., Gray, R.A., Challenor, P., Clayton, R.H., 2016. Uncertainty and variability in computational and mathematical models of cardiac physiology. J. Physiol. 594, 6833–6847.

Moore, J.W., Hines, M., Harris, E.M., 1984. Compensation for resistance in series with excitable membranes. Biophysical journal 46, 507–14.

Neher, E., 1992. [6] Correction for liquid junction potentials in patch clamp experiments, in: Methods in Enzymology. Academic Press. volume 207 of *Ion Channels*, pp. 123–131.

Neher, E., 1995. Voltage offsets in patch-clamp experiments, in: Sakmann, B., Neher, E. (Eds.), Single-Channel Recording. Springer US, Boston, MA. chapter 6, 2 edition. pp. 147–153.

Ng, C.A., Perry, M.D., Liang, W., Smith, N.J., Foo, B., Shrier, A., Lukacs, G.L., Hill, A.P., Vandenberg, J.I., 2019. High-throughput phenotyping of heteromeric human ether-à-go-go-related gene potassium channel variants can discriminate pathogenic from rare benign variants. Heart rhythm .

Niederer, S.A., Lumens, J., , Trayanova, N.A., 2018. Computational models in cardiology. Nat. Rev. Cardiol. 16, 100–111.

O'Hara, T., Virág, L., Varró, A., Rudy, Y., 2011. Simulation of the undiseased human cardiac ventricular action potential: model formulation and experimental validation. PLoS computational biology 7, e1002061.

Pathmanathan, P., Shotwell, M.S., Gavaghan, D.J., Cordeiro, J.M., Gray, R.A., 2015. Uncertainty quantification of fast sodium current steady-state inactivation for multi-scale models of cardiac electrophysiology. Progress in biophysics and molecular biology 117, 4–18.

Santillo, S., Moriello, A.S., Di Maio, V., 2014. Electrophysiological variability in the SH-SY5Y cellular line. Gen. Physiol. Biophys 33, 121–129.

Schmitt, B.M., Koepsell, H., 2002. An improved method for real-time monitoring of membrane capacitance in Xenopus laevis oocytes. Biophysical journal 82, 1345–1357.

Sherman, A.J., Shrier, A., Cooper, E., 1999. Series Resistance Compensation for Whole-Cell Patch-Clamp Studies Using a Membrane State Estimator. Biophysical Journal 77, 2590–2601.

Sigworth, F., 1995a. Design of the EPC-9, a computer-controlled patch-clamp amplifier. 1. Hardware. Journal of Neuroscience Methods 56, 195–202.

Sigworth, F., 1995b. Electronic design of the patch clamp, in: Sakmann, B., Neher, E. (Eds.), Single-Channel Recording. Springer US, Boston, MA. chapter 6, 2 edition. pp. 95–127.

Sigworth, F., Affolter, H., Neher, E., 1995. Design of the EPC-9, a computer-controlled patch-clamp amplifier. 2. Software. Journal of Neuroscience Methods 56, 203–215.

Strickholm, A., 1995. A single electrode voltage, current-and patch-clamp amplifier with complete stable series resistance compensation. Journal of Neuroscience Methods 61, 53–66.

Ten Tusscher, K., Noble, D., Noble, P.J., Panfilov, A.V., 2004. A model for human ventricular tissue. American Journal of Physiology-Heart and Circulatory Physiology 286, H1573–H1589.

Vandenberg, J.I., Varghese, A., Lu, Y., Bursill, J.A., Mahaut-Smith, M.P., Huang, C.L.H., 2006. Temperature dependence of human ether-a-go-go-related gene K+ currents. American Journal of Physiology-Cell Physiology 291, C165–75.

Weerakoon, P., Culurciello, E., Klemic, K.G., Sigworth, F.J., 2009. An Integrated Patch-Clamp Potentiostat With Electrode Compensation. IEEE Transactions on Biomedical Circuits and Systems 3, 117–125.

Weerakoon, P., Culurciello, E., Yang, Y., Santos-Sacchi, J., Kindlmann, P.J., Sigworth, F.J., 2010. Patch-clamp amplifiers on a chip. Journal of neuroscience methods 192, 187–92.

Zhou, Z., Gong, Q., Ye, B., Fan, Z., Makielski, J.C., Robertson, G.A., January, C.T., 1998. Properties of HERG channels stably expressed in HEK293 cells studied at physiological temperature. Biophysical Journal 74, 230–241.